Imaging bacterial peptidoglycan with near-infrared fluorogenic azide probes

Peyton Shieh[a], M. Sloan Siegrist[a], Andrew J. Cullen[a], and Carolyn R. Bertozzi[a,b,c,1]

Departments of [a]Chemistry and [b]Molecular and Cell Biology and [c]Howard Hughes Medical Institute, University of California, Berkeley, CA 94720

Edited by David A. Tirrell, California Institute of Technology, Pasadena, CA, and approved March 4, 2014 (received for review December 5, 2013)

Fluorescent probes designed for activation by bioorthogonal chemistry have enabled the visualization of biomolecules in living systems. Such activatable probes with near-infrared (NIR) emission would be ideal for in vivo imaging but have proven difficult to engineer. We present the development of NIR fluorogenic azide probes based on the Si-rhodamine scaffold that undergo a fluorescence enhancement of up to 48-fold upon reaction with terminal or strained alkynes. We used the probes for mammalian cell surface imaging and, in conjunction with a new class of cyclooctyne D-amino acids, for visualization of bacterial peptidoglycan without the need to wash away unreacted probe.

Bioorthogonal chemistry has created new opportunities for interrogating biomolecules in cells and organisms [for a general review of bioorthogonal chemistry, see Sletten and Bertozzi (1)]. For imaging studies, molecules tagged with a bioorthogonal reporter group can be detected with a fluorophore-conjugated reaction partner. Fluorogenic probes activated by these reactions can minimize fluorescence from excess probe. This attribute is particularly important in situations where washing is not possible, such as when imaging intracellular components or visualizing biomolecules in vivo.

Significant progress has been made in the discovery of fluorogenic probes activated by various bioorthogonal chemistries, including the Staudinger ligation (2, 3) as well as azide-alkyne (4–15) [for a review on fluorogenic probes activated by the azide-alkyne [3+2] cycloaddition, see Le Droumaguet et al. (4)], tetrazine-alkene (16–18), tetrazine-alkyne (19), and photoactivated tetrazole-alkene cycloadditions (20, 21). However, the dyes used have emission maxima below 600 nm. The identification of activatable near-infrared (NIR) fluorogenic probes, with emission maxima approaching 700 nm, has proven much more challenging. These longer wavelengths are ideal for interrogating biological systems, as background autofluorescence is minimized and tissue penetrance is highest. There have been a few reports of such long-wavelength fluorogenic probes activated by bioorthogonal chemistry. For example, the reaction of tetrazine-conjugated DyLight650 with a cyclooctyne analog formed a product that was 1.6-fold brighter than the starting material (22). Likewise, weakly fluorescent long-wavelength pyrazolines can be generated by the photoactivated tetrazole-alkene cycloaddition of nonfluorescent substrates (23). Brighter NIR dyes with more dramatic fluorescence enhancements are desirable for applications of bioorthogonal chemistry to biological imaging.

Recently, Xiao, Nagano, and their respective co-workers (24, 25) found that replacement of the oxygen atom in the xanthene moiety of tetramethylrhodamine with a silicon atom (Si-rhodamine) induces a dramatic red shift in emission of nearly 100 nm into the NIR region. Importantly, the fluorescence quantum yields of these probes could be modulated by over 100-fold through photoinduced electron transfer (PeT), rendering Si-rhodamine a promising scaffold for sensor development (26–28). Additionally, carboxy-substituted Si-rhodamines are well suited for cell labeling due to spirolactonization and loss of fluorescence during nonspecific binding events (29).

We sought to identify azide-functionalized Si-rhodamines that would undergo a significant enhancement in fluorescence quantum yield upon triazole formation. In previous work, we used PeT from the pendant aryl ring to control the fluorescence quantum yield of fluorogenic azidofluoresceins (30). Conversion of their aryl azides to the corresponding triazoles upon Cu-catalyzed or copper-free "click" reaction with alkynes decreased their aryl ring electron density, which reduced PeT efficiency and resulted in fluorescence enhancement. Using computational methods, we identified azidofluorescein analogs that were likely to be highly fluorogenic upon alkyne cycloaddition. Because Nagano and co-workers have shown that Si-rhodamines are amenable to the same kinds of computational predictions, we reasoned that these NIR dyes might be engineered to respond to bioorthogonal chemistries (Fig. 1).

Here, we present a series of fluorogenic azido Si-rhodamine probes with emission maxima near 670 nm and up to 48-fold enhancement in fluorescence quantum yield upon triazole formation. Further optimization of these probes yielded compounds that were suitable for the detection of terminal alkynes on mammalian cell surfaces without the need to remove excess probe, i.e., "no-wash" labeling. Use of these optimized probes in conjunction with a new class of cyclooctyne D-amino acids allowed for the no-wash visualization of bacterial peptidoglycan (PG) using biocompatible copper-free click chemistry. This work therefore establishes a platform for the in vivo imaging of bacterial pathogens.

Results and Discussion

Synthesis and Evaluation of Azido Si-Rhodamines. We developed an efficient and modular synthesis to access azide-functionalized Si-rhodamines from various bromoanilines (Fig. 2). The bromoanilines were first protected as the bis-trimethylsilyl (TMS) derivatives by

Significance

Bioorthogonal chemistry has created new opportunities for interrogating biomolecules in cells and organisms. Near-infrared (NIR) fluorogenic probes activated by bioorthogonal chemistry are ideal for imaging studies, as tissue penetrance is highest and background fluorescence from excess probe and endogenous biomolecules is minimized at these wavelengths. Here, we present the development and optimization of NIR fluorogenic azide probes that undergo a fluorescence enhancement of up to 48-fold upon reaction with terminal or strained alkynes. In conjunction with a new class of cyclooctyne D-amino acids, the NIR probes were used to image bacterial peptidoglycan (PG) without the need for cytotoxic copper catalyst or washing away excess probe. This platform should facilitate the in vivo imaging of PG in pathogenic bacteria with bioorthogonal chemistry.

Author contributions: P.S., M.S.S., and C.R.B. designed research; P.S. and A.J.C. performed research; P.S., M.S.S., and C.R.B. analyzed data; and P.S., M.S.S., and C.R.B. wrote the paper.

The authors declare no conflict of interest.

This article is a PNAS Direct Submission.

[1]To whom correspondence should be addressed. E-mail: crb@berkeley.edu.

This article contains supporting information online at www.pnas.org/lookup/suppl/doi:10.1073/pnas.1322727111/-/DCSupplemental.

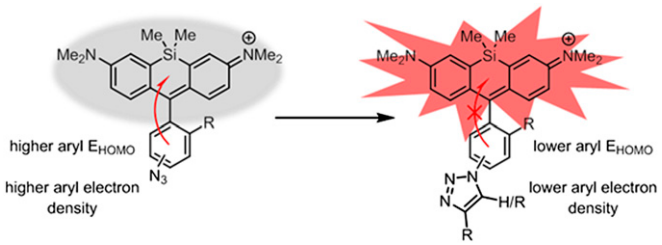

Fig. 1. Design of a PeT-based fluorogenic azido Si-rhodamine.

deprotonation with lithium hexamethyldisilazide (LiHMDS) and reaction with trimethylsilyl chloride (TMSCl). Next, the protected bromoanilines were subjected to lithium–halogen exchange and added into Si-xanthone, which afforded the amino Si-rhodamines after acidic workup. As described later, the photophysical properties of these intermediates were measured in comparison with their azido and triazolyl counterparts. The amino Si-rhodamines were finally subjected to diazotization with sodium nitrite and displacement by azide ion to yield the desired azido Si-rhodamines. Through this route, we generated compounds **1–9** (Fig. 3). To evaluate fluorescence enhancement upon triazole formation, we also synthesized the corresponding triazolyl Si-rhodamines by copper-catalyzed click chemistry with 4-pentynoyl ethanolamine amide (compound **A**, Fig. 2).

The fluorescence quantum yields of the purified amino, azido, and triazolyl Si-rhodamines were measured in pH 7.4 PBS using cresyl violet in methanol (Φ_{fl} = 0.54) as a standard (Table 1). The four analogs containing the same pendant aryl rings from our previous study (30) (**1** to **4**, Fig. 3) did not display significant fluorescence enhancement upon triazole formation. The best candidate of the four, 8-azidonaphthyl–substituted Si-rhodamine **1**, afforded only a 5-fold increase in fluorescence quantum yield compared with the 29-fold enhancement we observed with the corresponding fluorescein (30). This result was not unexpected given the difference in electronics between the two systems and Nagano and co-workers' previous observation that more electron-rich pendant aryl rings are needed to quench fluorescence via PeT in Si-rhodamines (27).

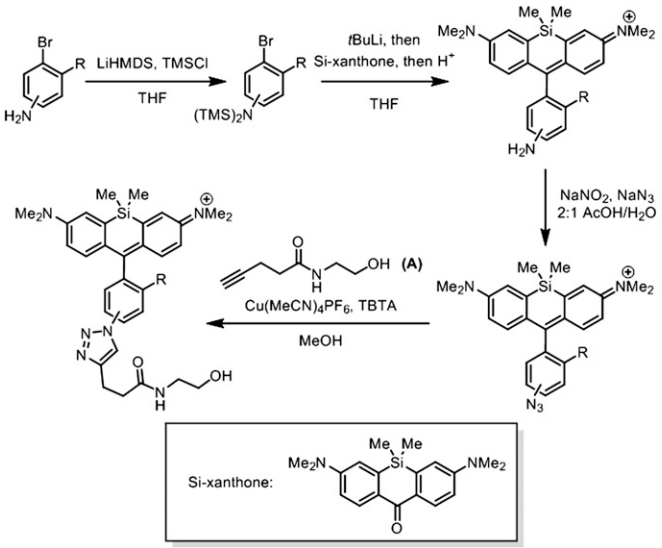

Fig. 2. Synthesis of amino, azido and triazolyl Si-rhodamines from bromoanilines. TBTA, tris[(1-benzyl-1*H*-1,2,3-triazol-4-yl)methyl]amine; *t*BuLi, *tert*-butyl lithium.

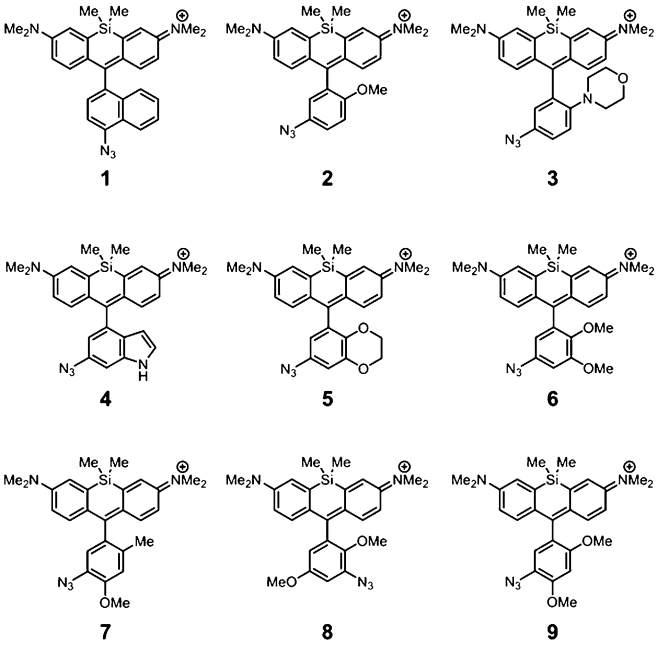

Fig. 3. Structures of azido Si-rhodamines synthesized and evaluated.

Computational results suggested that the pendant aryl rings of compounds **5–9** possess higher electron density than that of compound **1** (*SI Appendix*, Fig. S1). We therefore synthesized these compounds and characterized their photophysical properties experimentally (Table 1). 3-Azido-4,6-dimethoxy-Si-rhodamine **9** (Fig. 3), the most promising of this group, displayed a 48-fold increase in fluorescence quantum yield upon triazole formation. This fluorescence enhancement was recapitulated in situ by monitoring fluorescence immediately after addition of alkyne **A** to a solution of $CuSO_4$, the ligand 2-[4-({bis[(1-*tert*-butyl-1*H*-1,2,3-triazol-4-yl)methyl]amino}methyl)-1*H*-1,2,3-triazol-1-yl]acetic acid (BTTAA) (31), sodium ascorbate, and compound **9** (Fig. 4). Under these conditions, the absorption of the compound did not change significantly (*SI Appendix*, Fig. S2), indicating that the observed change in fluorescence intensity arises solely from an increase in fluorescence quantum yield.

An interesting feature of compounds **1–9** is that their fluorescence quantum yields, which are already lower than those of the corresponding triazoles, are even further reduced by conversion to the corresponding amines (Table 1), a potential route of biological degradation (32). Thus, azide reduction, if it occurs, will suppress rather than enhance background fluorescence for this set of azido Si-rhodamine probes. This property stands in contrast to probes where azide reduction is a key part of sensor design (33–35). Although a trend exists between calculated E_{HOMO} and fluorescence quantum yield for compounds **1–9** (*SI Appendix*, Fig. S3), the observed differences in quantum yields for some compounds with similar E_{HOMO}s (for example, compare the data for compounds **8** and **9** in Table 1) suggest that other factors might influence PeT efficiency, or that other fluorescence quenching mechanisms are at play.

Optimization of Azido Si-Rhodamine 9 for Mammalian Cell Surface Labeling. We tested compound **9** as a biological imaging reagent using mammalian cells that had been metabolically labeled with peracetylated *N*-pentynoylmannosamine (Ac_4ManNAl), which is metabolized to *N*-pentynoyl sialic acid (SiaNAl) and presented on cell surface glycoconjugates (36, 37). However, compound **9** showed significant alkyne-independent background labeling even after repeated washing steps, most likely due to its substantial

Table 1. Photophysical properties of Si-rhodamines 1–9 and their amino and triazolyl counterparts in PBS, pH 7.4

Compound	λ_{abs}, nm	λ_{em}, nm	Φ_{fl}	Change in Φ_{fl}
1-NH_2	653	669	0.0016	24-fold ↓
1-N_3	654	666	0.038	—
1-triazole	656	670	0.19	5.0-fold ↑
2-NH_2	650	669	0.0025	32-fold ↓
2-N_3	653	667	0.081	—
2-triazole	655	669	0.19	2.3-fold ↑
3-NH_2	650	672	0.00096	1.4-fold ↓
3-N_3	656	667	0.0014	—
3-triazole	663	676	0.0015	1.1-fold ↑
4-NH_2	650	673	0.00088	5.5-fold ↓
4-N_3	660	669	0.0048	—
4-triazole	654	668	0.0088	1.8-fold ↑
5-NH_2	653	667	0.00093	21-fold ↓
5-N_3	655	668	0.019	—
5-triazole	656	668	0.18	9.5-fold ↑
6-NH_2	652	665	0.00067	58-fold ↓
6-N_3	654	669	0.039	—
6-triazole	656	670	0.18	4.6-fold ↑
7-NH_2	648	669	0.0015	45-fold ↓
7-N_3	650	666	0.066	—
7-triazole	652	666	0.25	3.7-fold ↑
8-NH_2	654	672	0.0012	41-fold ↓
8-N_3	655	669	0.051	—
8-triazole	657	671	0.16	3.2-fold ↑
9-NH_2	650	664	0.0014	3.0-fold ↓
9-N_3	654	666	0.0042	—
9-triazole	655	668	0.20	48-fold ↑

hydrophobic character. We hypothesized that replacing the methoxy groups with more water-soluble alkoxy substituents would maintain the electronic balance between the pendant aryl and the Si-xanthene moieties while enhancing hydrophilicity. To this end, we synthesized compound **10** in six steps from 2,4-difluoronitrobenzene (Fig. 5 and *SI Appendix*, Scheme S1). Consistent with our hypothesis, compound **10** underwent a significant fluorescence enhancement upon copper-catalyzed click reaction with alkyne **A** (*SI Appendix*, Fig. S4).

We next evaluated Si-rhodamine **10** as a reagent for imaging SiaNAl residues on live cell surfaces. CHO K1 cells were incubated with 50 μM Ac_4ManNAl for 3 d, washed, and then incubated with 5 μM **10**, 50 μM $CuSO_4$, 300 μM BTTAA, and 1 mM sodium ascorbate. After 15 min, without washing away excess probe, we observed robust cell surface labeling (*SI Appendix*, Fig. S5). We were also able to visualize cell surface glycan labeling as it occurred in real time (*SI Appendix*, Fig. S6). Gratifyingly, background labeling was minimal on control cells treated with *N*-acetylmannosamine (Ac_4ManNAc) (*SI Appendix*, Fig. S5).

When we performed a similar experiment using HEK 293T cells, punctate fluorescence appeared within the cells almost immediately after exposure compound **10** (*SI Appendix*, Fig. S7). It has been previously demonstrated that Si-rhodamines, as lipophilic cations, can localize to the mitochondria (25). Indeed, such localization of our probe was confirmed by costaining with Mitotracker Green (*SI Appendix*, Fig. S8). This observation suggests that, although probe **10** has the potentially beneficial property of cell permeability, it may be compromised by unwanted mitochondrial labeling in some eukaryotic cell types.

To prevent mitochondrial labeling, we synthesized bis-sulfated probe **11**, anticipating that the negative charges would limit cell permeability as well as mitochondrial localization (Fig. 5 and *SI Appendix*, Scheme S2). Like its predecessors, compound **11** displayed significant fluorescence enhancement upon triazole formation (*SI Appendix*, Fig. S9). In contrast to compound **10**, this bis-sulfated probe gave robust cell surface labeling under no-wash conditions for both CHO K1 and HEK 293T cells, with no unwanted background or mitochondrial labeling (Fig. 6 and *SI Appendix*, Fig. S10).

Incorporation of Cyclooctyne-Functionalized D-Alanine Analogs into PG. Bacterial PG is an emerging target for molecular imaging using bioorthogonal chemistry (38–43). We and others have shown

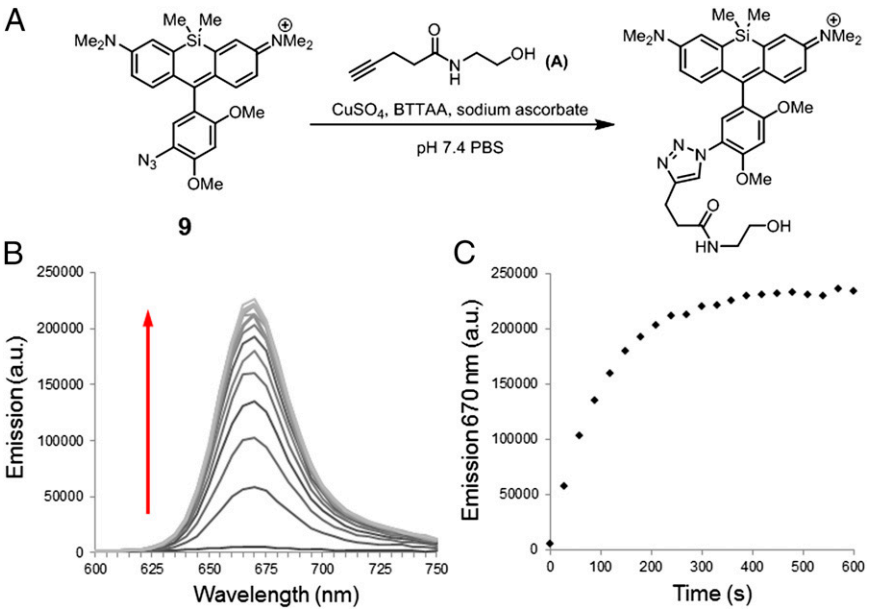

Fig. 4. Fluorescence enhancement of **9** during copper-catalyzed click reaction in situ. (*A*) The reaction between fluorogenic Si-rhodamine **9** and alkyne **A**. (*B*) Emission spectra acquired during the reaction. Scans were performed every 30 s, with the first scan acquired immediately before addition of alkyne **A**. λ_{ex} = 600 nm. (*C*) Plot of emission at 670 nm vs. reaction time.

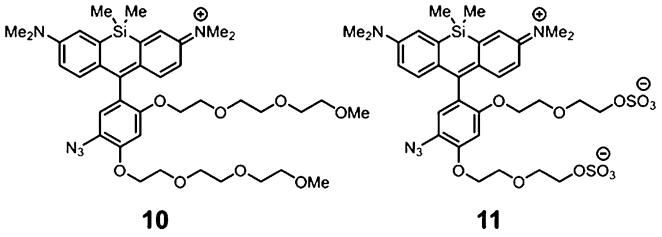

Fig. 5. Structures of bis-oligoethylene glycol-substituted azido Si-rhodamine probe **10** and bis-sulfated probe **11**.

that D-alanine analogs adorned with various side-chain functionalities can be incorporated into the peptide portion of PG in a variety of bacterial species (40, 41). Metabolic labeling with an alkyne-functionalized D-alanine derivative (alkDala), for example, allowed fluorescence imaging of PG by copper-catalyzed click chemistry with azide-functionalized probes (40, 41). The promiscuity of PG metabolic enzymes toward both natural and unnatural D-amino acid substrates suggested that incorporation of the relatively large cyclooctyne moiety might be possible (40, 41, 44–46). If so, metabolic labeling with a cyclooctyne D-alanine analog would enable copper-free PG imaging using the NIR fluorogenic probes described above.

Accordingly, we synthesized cyclooctyne-functionalized D-alanine analog **12** (octDala) as well as the bicyclononyne (BCN)-derivatized stereoisomers **13** (exobcnDala) and **14** (endobcnDala), all in two steps from known compounds (47–49) (Fig. 7*A* and *SI Appendix*, Scheme S3). The minimally substituted cyclooctyne ring of **12** offers the least steric bulk, but is less reactive than the BCN moiety of **13** and **14** (49). Although there are other means of enhancing cyclooctyne reactivity, such as aryl ring fusions (50), these would impose much additional steric bulk.

We tested the metabolic incorporation of **12–14** into the cell walls of the Gram-positive bacteria *Mycobacterium smegmatis*, *Corynebacterium glutamicum*, and *Listeria monocytogenes*. The bacteria were grown for one doubling time in the presence of 5 mM **12**, **13**, or **14**, washed to remove excess amino acid, and then reacted with 20 μM commercially available azido-PEG_3-carboxyrhodamine 110, a reagent we previously used to image alkDala-labeled PG under copper-catalyzed conditions (40). The cells were washed to remove excess probe, fixed, and analyzed by flow cytometry and microscopy (*SI Appendix*, Figs. S11–S13). The fluorescence intensities observed correlated with the relative reactivities of the parent cyclooctynes. Cells incubated with **13** and **14** followed by copper-free reaction with azido-PEG_3-carboxyrhodamine 110 showed comparable fluorescence intensity to cells metabolically labeled with alkDala followed by copper-catalyzed reaction with the same probe. Thus, cyclooctyne D-alanine analogs **13** and **14** enable PG imaging with the same sensitivity as the earlier methods, but without the need for a cytotoxic copper catalyst.

Although the observed fluorescence appeared to concentrate at the bacterial cell walls (*SI Appendix*, Figs. S11–S13), consistent with incorporation of cyclooctyne D-alanine analogs into PG, we sought additional evidence that these unnatural amino acids access the same metabolic pathways as natural D-alanine. We performed a competition experiment showing that excess D-alanine decreases the fluorescence intensity of *L. monocytogenes* incubated with **12**, **13**, or **14** (*SI Appendix*, Fig. S14). Additionally, we found that *L. monocytogenes* lacking the PBP5 carboxypeptidase (51), which trims the terminal D-alanine residues from the pentapeptide PG crosslink, shows enhanced labeling compared with wild-type bacteria (*SI Appendix*, Fig. S15). The labeling enhancement in the absence of PBP5 is comparable for both the relatively small alkDala and our bulkier cyclooctyne amino acids, suggesting that this carboxypeptidase is tolerant of larger, unnatural D-amino acids.

Copper-Free PG Imaging with Fluorogenic NIR Azide Probes. Finally, we imaged the bacteria using our NIR fluorogenic azide probes. We first confirmed that azido Si-rhodamines **9**, **10**, and **11** would undergo an enhancement in fluorescence upon reaction with cyclooctynes. These probes were incubated with endo-bicyclononynol in vitro to generate triazole products (*SI Appendix*, Fig. S16*A*). Their fluorescence enhancement was similar to that observed in the copper-catalyzed click reaction with linear alkynes, showing that the fluorogenic character of probes **9–11** is not dependent on the substitution pattern of the triazole (*SI Appendix*, Fig. S16*B*). All three bacterial species were incubated with endobcnDala **14** as before, but after washing away excess amino acid, the bacteria were incubated with 10 or 20 μM **11** for 1 h and directly imaged without washing away excess probe (Fig. 7*B*). Clear fluorescence signal over background was observed in all cases, demonstrating the suitability of cyclooctyne-functionalized D-amino acids and fluorogenic azides for imaging PG on

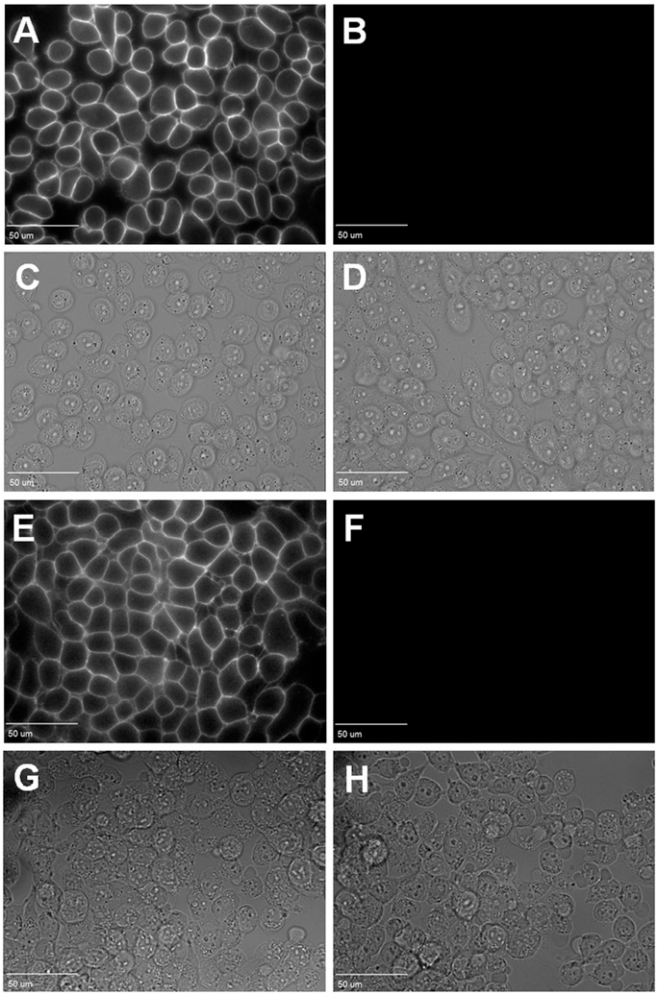

Fig. 6. No-wash mammalian cell surface labeling with bis-sulfated probe **11**. (*A* and *C*) Fluorescence and bright-field images of CHO K1 cells treated with Ac_4ManNAl and labeled with **11**. (*B* and *D*) Fluorescence and bright-field images of CHO K1 cells treated with Ac_4ManNAc and labeled with **11**. (*E* and *G*) Fluorescence and bright-field images of HEK 293T cells treated with Ac_4ManNAl and labeled with **11**. (*F* and *H*) Fluorescence and bright-field images of HEK 293T cells treated with Ac_4ManNAc and labeled with **11**. (Scale bar: 50 μm.)

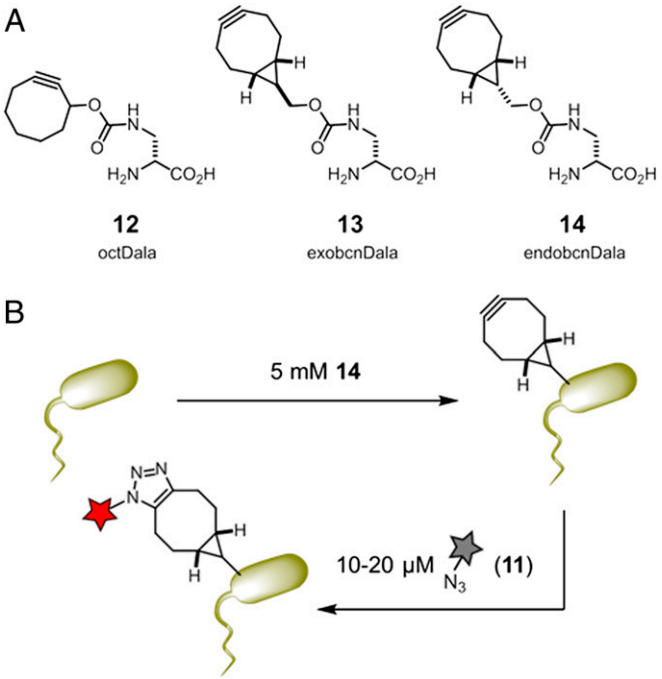

Fig. 7. Imaging bacterial PG with cyclooctyne D-alanine analogs and fluorogenic azide probes. (*A*) Structures of cyclooctyne D-amino acids **12** through **14**. (*B*) No-wash PG labeling workflow using endobcnDala **14** and bis-sulfated azido Si-rhodamine **11**.

live cells (Fig. 8). Notably, cyclooctyne-dependent labeling was observable even with the use of 500 μM endobcnDala **14**, showing that the sensitivity of our method can be comparable to other D-amino acid labeling strategies (*SI Appendix*, Fig. S17). Although the biosynthetic machinery can tolerate fluorophore-conjugated D-amino acids, allowing one-step PG imaging versus our two-step metabolic/chemical labeling approach, chemical reporter groups are much smaller than long-wavelength fluorophores and therefore minimize possible biological perturbations (41). The Gram-negative organism *Escherichia coli* metabolized compound **14** similarly to the Gram-positive bacteria, but was not efficiently labeled with dye **11** (*SI Appendix*, Fig. S18). We hypothesize that the presence of an outer membrane (although apparently not a mycobacterial "mycomembrane"; Fig. 8 *A–D*) limits access of compound **11** to PG. By contrast, smaller dyes were able to access both terminal alkynes (40) and cyclooctynes in metabolically labeled *E. coli* PG (*SI Appendix*, Fig. S19).

Conclusions

In summary, we present the development of fluorogenic NIR azide probes with up to 48-fold enhancement in fluorescence upon triazole formation. Derivatives with improved water solubility enabled no-wash NIR imaging of glycoconjugates on live mammalian cells. Our modular synthesis of Si-rhodamine analogs with variously substituted pendant aryl rings allows facile modification of their physical and biochemical properties while maintaining a significant fluorescence enhancement. Additionally, we found that the bacterial PG biosynthetic machinery tolerates D-alanine analogs bearing cyclooctynes. Together with the fluorogenic NIR probes, this finding enabled us to image PG in several bacterial species under nontoxic copper-free conditions and without the need to wash away excess fluorescent probe. This platform should facilitate the in vivo imaging of PG in pathogenic bacteria, either in cultured host cells or model organisms, with bioorthogonal chemistry.

More broadly, there has been much recent effort toward the delivery of cyclooctyne chemical reporters into various cellular

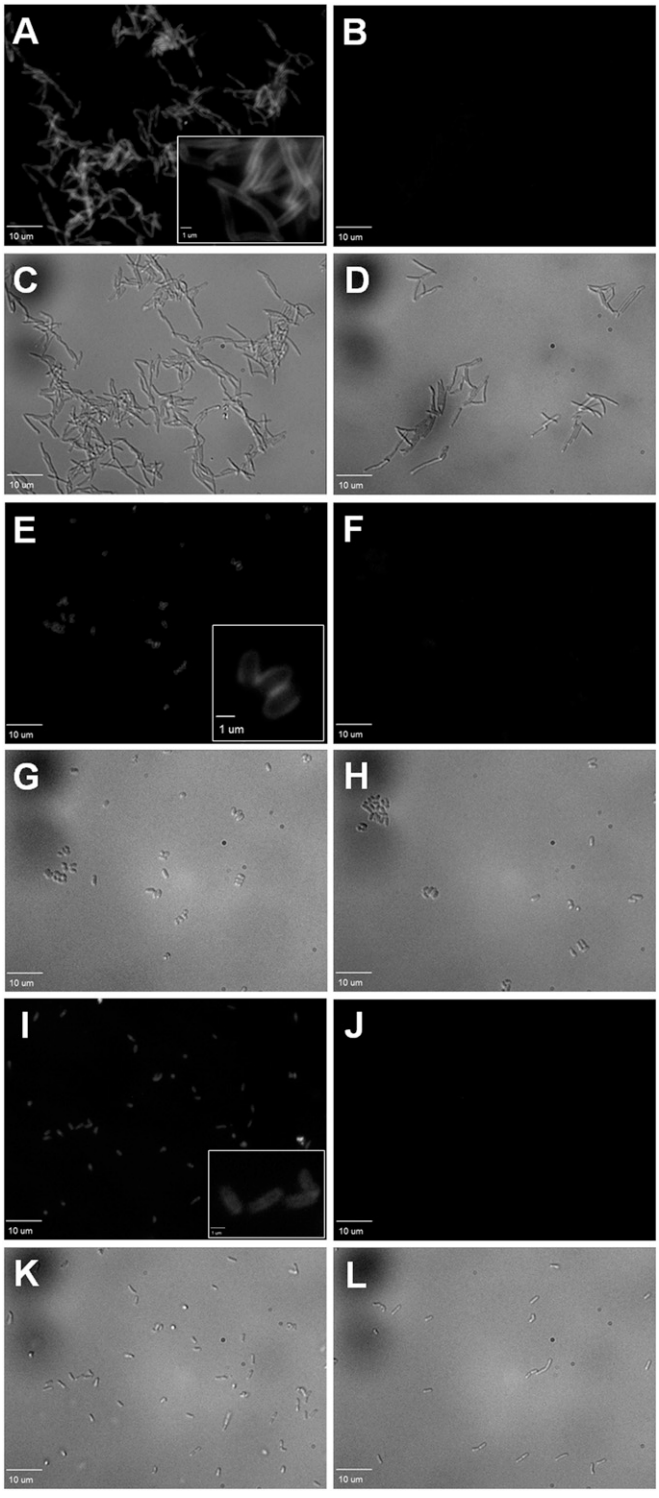

Fig. 8. No-wash bacterial PG labeling. Bacteria were treated with 5 mM endobcnDala **14** or D-alanine, and then reacted with 10 or 20 μM bis-sulfated probe **11** for 1 h. (*A–D*) Fluorescence and bright-field images of *M. smegmatis* treated with **14** or D-alanine and labeled with 10 μM **11**. (*E–H*) Fluorescence and bright-field images of *C. glutamicum* treated under the same conditions. (*I–L*) Fluorescence and bright-field images of *L. monocytogenes pbp::tn* treated under the same conditions, but labeled with 20 μM **11**. (Scale bar: 10 μm.) *Insets* in *A*, *E*, and *I* show cells enlarged to highlight cell surface labeling. (Scale bar: 1 μm.)

biopolymers. Site-specific incorporation of cyclooctynes into proteins has been accomplished via the pyrrolysine system (19, 48, 52), for example, and cyclooctynes can be integrated into cell surface lipid structures as well (53). The fluorogenic azide dyes reported here should augment applications of these other experimental platforms.

ACKNOWLEDGMENTS. We thank Prof. C. Chang (University of California, Berkeley) for the generous use of his UV/vis spectrophotometer and fluorometer. We also thank A. Aditham for assistance with biological experiments and A. Aron for assistance in the synthesis of **12**. This work was funded by National Institutes of Health Grants GM058867 and AI051622 (to C.R.B.). M.S.S. was supported by a postdoctoral fellowship from the American Cancer Society (119087-PF-10-258-01-MPC).

1. Sletten EM, Bertozzi CR (2009) Bioorthogonal chemistry: Fishing for selectivity in a sea of functionality. *Angew Chem Int Ed Engl* 48(38):6974–6998.
2. Lemieux GA, De Graffenried CL, Bertozzi CR (2003) A fluorogenic dye activated by the staudinger ligation. *J Am Chem Soc* 125(16):4708–4709.
3. Hangauer MJ, Bertozzi CR (2008) A FRET-based fluorogenic phosphine for live-cell imaging with the Staudinger ligation. *Angew Chem Int Ed Engl* 47(13):2394–2397.
4. Le Droumaguet C, Wang C, Wang Q (2010) Fluorogenic click reaction. *Chem Soc Rev* 39(4):1233–1239.
5. Sivakumar K, et al. (2004) A fluorogenic 1,3-dipolar cycloaddition reaction of 3-azidocoumarins and acetylenes. *Org Lett* 6(24):4603–4606.
6. Xie F, et al. (2008) A fluorogenic "click" reaction of azidoanthracene derivatives. *Tetrahedron* 64(13):2906–2914.
7. Wang C, Xie F, Suthiwangcharoen N, Sun J, Wang Q (2012) Tuning the optical properties of BODIPY dye through Cu(I) catalyzed azide-alkyne cycloaddition (CuAAC) reaction. *Sci China Chem* 55(1):125–130.
8. Sawa M, et al. (2006) Glycoproteomic probes for fluorescent imaging of fucosylated glycans in vivo. *Proc Natl Acad Sci USA* 103(33):12371–12376.
9. Zhou Z, Fahrni CJ (2004) A fluorogenic probe for the copper(I)-catalyzed azide-alkyne ligation reaction: Modulation of the fluorescence emission via 3(n,pi)-1(pi,pi) inversion. *J Am Chem Soc* 126(29):8862–8863.
10. Jewett JC, Bertozzi CR (2011) Synthesis of a fluorogenic cyclooctyne activated by Cu-free click chemistry. *Org Lett* 13(22):5937–5939.
11. Key JA, Cairo CW (2011) Identification of fluorogenic and quenched benzoxadiazole reactive chromophores. *Dyes Pigments* 88(1):95–102.
12. Qi J, Han MS, Chang YC, Tung CH (2011) Developing visible fluorogenic "click-on" dyes for cellular imaging. *Bioconjug Chem* 22(9):1758–1762.
13. Li J, Hu M, Yao SQ (2009) Rapid synthesis, screening, and identification of xanthone- and xanthene-based fluorophores using click chemistry. *Org Lett* 11(14):3008–3011.
14. Friscourt F, Fahrni CJ, Boons GJ (2012) A fluorogenic probe for the catalyst-free detection of azide-tagged molecules. *J Am Chem Soc* 134(45):18809–18815.
15. Herner A, Nikić I, Kállay M, Lemke EA, Kele P (2013) A new family of bioorthogonally applicable fluorogenic labels. *Org Biomol Chem* 11(20):3297–3306.
16. Devaraj NK, Hilderbrand S, Upadhyay R, Mazitschek R, Weissleder R (2010) Bioorthogonal turn-on probes for imaging small molecules inside living cells. *Angew Chem Int Ed Engl* 49(16):2869–2872.
17. Lang K, et al. (2012) Genetically encoded norbornene directs site-specific cellular protein labelling via a rapid bioorthogonal reaction. *Nat Chem* 4(4):298–304.
18. Carlson JCT, Meimetis LG, Hilderbrand SA, Weissleder R (2013) BODIPY-tetrazine derivatives as superbright bioorthogonal turn-on probes. *Angew Chem Int Ed Engl* 52(27):6917–6920.
19. Lang K, et al. (2012) Genetic encoding of bicyclononynes and trans-cyclooctenes for site-specific protein labeling in vitro and in live mammalian cells via rapid fluorogenic Diels-Alder reactions. *J Am Chem Soc* 134(25):10317–10320.
20. Wang Y, Song W, Hu WJ, Lin Q (2009) Fast alkene functionalization in vivo by photoclick chemistry: HOMO lifting of nitrile imine dipoles. *Angew Chem Int Ed Engl* 48(29):5330–5333.
21. Yu Z, Ho LY, Lin Q (2011) Rapid, photoactivatable turn-on fluorescent probes based on an intramolecular photoclick reaction. *J Am Chem Soc* 133(31):11912–11915.
22. Neves AA, et al. (2013) Imaging cell surface glycosylation in vivo using "double click" chemistry. *Bioconjug Chem* 24(6):934–941.
23. An P, Yu Z, Lin Q (2013) Design and synthesis of laser-activatable tetrazoles for a fast and fluorogenic red-emitting 1,3-dipolar cycloaddition reaction. *Org Lett* 15(21):5496–5499.
24. Fu M, Xiao Y, Qian X, Zhao D, Xu Y (2008) A design concept of long-wavelength fluorescent analogs of rhodamine dyes: Replacement of oxygen with silicon atom. *Chem Commun (Camb)* 2008(15):1780–1782.
25. Koide Y, Urano Y, Hanaoka K, Terai T, Nagano T (2011) Evolution of group 14 rhodamines as platforms for near-infrared fluorescence probes utilizing photoinduced electron transfer. *ACS Chem Biol* 6(6):600–608.
26. Koide Y, Urano Y, Hanaoka K, Terai T, Nagano T (2011) Development of an Si-rhodamine-based far-red to near-infrared fluorescence probe selective for hypochlorous acid and its applications for biological imaging. *J Am Chem Soc* 133(15):5680–5682.
27. Egawa T, et al. (2011) Development of a far-red to near-infrared fluorescence probe for calcium ion and its application to multicolor neuronal imaging. *J Am Chem Soc* 133(36):14157–14159.
28. Wang T, et al. (2012) Spirolactonized Si-rhodamine: A novel NIR fluorophore utilized as a platform to construct Si-rhodamine-based probes. *Chem Commun (Camb)* 48(70):8781–8783.
29. Lukinavičius G, et al. (2013) A near-infrared fluorophore for live-cell super-resolution microscopy of cellular proteins. *Nat Chem* 5(2):132–139.
30. Shieh P, Hangauer MJ, Bertozzi CR (2012) Fluorogenic azidofluoresceins for biological imaging. *J Am Chem Soc* 134(42):17428–17431.
31. Besanceney-Webler C, et al. (2011) Increasing the efficacy of bioorthogonal click reactions for bioconjugation: A comparative study. *Angew Chem Int Ed Engl* 50(35):8051–8056.
32. Staros JV, Bayley H, Standring DN, Knowles JR (1978) Reduction of aryl azides by thiols: Implications for the use of photoaffinity reagents. *Biochem Biophys Res Commun* 80(3):568–572.
33. Lin VS, Chang CJ (2012) Fluorescent probes for sensing and imaging biological hydrogen sulfide. *Curr Opin Chem Biol* 16(5-6):595–601.
34. Lord SJ, et al. (2008) A photoactivatable push-pull fluorophore for single-molecule imaging in live cells. *J Am Chem Soc* 130(29):9204–9205.
35. Lee HL, et al. (2010) Superresolution imaging of targeted proteins in fixed and living cells using photoactivatable organic fluorophores. *J Am Chem Soc* 132(43):15099–15101.
36. Hsu TL, et al. (2007) Alkynyl sugar analogs for the labeling and visualization of glycoconjugates in cells. *Proc Natl Acad Sci USA* 104(8):2614–2619.
37. Chang PV, et al. (2009) Metabolic labeling of sialic acids in living animals with alkynyl sugars. *Angew Chem Int Ed Engl* 48(22):4030–4033.
38. Nelson JW, et al. (2010) A biosynthetic strategy for re-engineering the *Staphylococcus aureus* cell wall with non-native small molecules. *ACS Chem Biol* 5(12):1147–1155.
39. Chung HJ, et al. (2011) Ubiquitous detection of gram-positive bacteria with bioorthogonal magnetofluorescent nanoparticles. *ACS Nano* 5(11):8834–8841.
40. Siegrist MS, et al. (2013) (D)-amino acid chemical reporters reveal peptidoglycan dynamics of an intracellular pathogen. *ACS Chem Biol* 8(3):500–505.
41. Kuru E, et al. (2012) In situ probing of newly synthesized peptidoglycan in live bacteria with fluorescent D-amino acids. *Angew Chem Int Ed Engl* 51(50):12519–12523.
42. Liechti GW, et al. (2014) A new metabolic cell-wall labelling method reveals peptidoglycan in *Chlamydia trachomatis*. *Nature* 506(7489):507–510.
43. Pilhofer M, et al. (2013) Discovery of chlamydial peptidoglycan reveals bacteria with murein sacculi but without FtsZ. *Nat Commun* 4(2856):1–7.
44. Caparrós M, Pisabarro AG, de Pedro MA (1992) Effect of D-amino acids on structure and synthesis of peptidoglycan in *Escherichia coli*. *J Bacteriol* 174(17):5549–5559.
45. Lam H, et al. (2009) D-amino acids govern stationary phase cell wall remodeling in bacteria. *Science* 325(5947):1552–1555.
46. Cava F, de Pedro MA, Lam H, Davis BM, Waldor MK (2011) Distinct pathways for modification of the bacterial cell wall by non-canonical D-amino acids. *EMBO J* 30(16):3442–3453.
47. Lau YH, Spring DR (2011) Efficient synthesis of Fmoc-protected azido amino acids. *Synlett* 2011(13):1917–1919.
48. Plass T, Milles S, Koehler C, Schultz C, Lemke EA (2011) Genetically encoded copper-free click chemistry. *Angew Chem Int Ed Engl* 50(17):3878–3881.
49. Dommerholt J, et al. (2010) Readily accessible bicyclononynes for bioorthogonal labeling and three-dimensional imaging of living cells. *Angew Chem Int Ed Engl* 49(49):9422–9425.
50. Jewett JC, Bertozzi CR (2010) Cu-free click cycloaddition reactions in chemical biology. *Chem Soc Rev* 39(4):1272–1279.
51. Guinane CM, Cotter PD, Ross RP, Hill C (2006) Contribution of penicillin-binding protein homologs to antibiotic resistance, cell morphology, and virulence of *Listeria monocytogenes* EGDe. *Antimicrob Agents Chemother* 50(8):2824–2828.
52. Borrmann A, et al. (2012) Genetic encoding of a bicyclo[6.1.0]nonyne-charged amino acid enables fast cellular protein imaging by metal-free ligation. *ChemBioChem* 13(14):2094–2099.
53. Neef AB, Schultz C (2009) Selective fluorescence labeling of lipids in living cells. *Angew Chem Int Ed Engl* 48(8):1498–1500.